# Siegert approach within a microscopic description of nucleus-nucleus bremsstrahlung

J. Dohet-Eraly* and D. Baye†

*Physique Quantique, C. P. 165/82, and Physique Nucléaire Théorique et Physique Mathématique, C. P. 229, Université Libre de Bruxelles (ULB), B-1050 Brussels, Belgium*

(Received 8 March 2013; revised manuscript received 10 June 2013; published 8 August 2013)

Previous studies of nucleus-nucleus bremsstrahlung within the microscopic cluster model made use of a simplified current version of the electric transition operators, neglecting the meson exchange currents. The present microscopic cluster model relies on operators based on the charge density derived from an extension of the Siegert theorem valid for arbitrary photon energy. A part of the meson exchange current effects is then implicitly included in this approach. Divergence problems in matrix elements are avoided. The model is applied to the $\alpha + \alpha$ system at low photon energy for which experimental data are available. In particular, good agreement is obtained with data about on- and off-resonance $4^+ \rightarrow 2^+$ transitions. The differences between the charge and current approaches are discussed on this example.

DOI: 10.1103/PhysRevC.88.024602 PACS number(s): 25.20.Lj, 24.30.−v, 21.60.Gx, 25.55.−e

## I. INTRODUCTION

The description of electromagnetic transitions has been a focus of interest in nuclear physics for a long time. Radiative transitions within the continuum, also called bremsstrahlung, were actively studied for nucleon-proton collisions [1–5] but more rarely for other types of collisions at low energies, and in particular in collisions between light ions. The energy of photons emitted in such low-energy nucleus-nucleus scattering is taken from the relative motion of the colliding nuclei. Measurements of bremsstrahlung cross sections involving light nuclei were performed mostly in the 1970s for proton-deuteron [6], proton-$\alpha$ [7–9], $\alpha$-$^3$He [10], and $\alpha$-$\alpha$ scatterings [10,11]. The data were rather scarce and restricted to a peculiar planar geometry. Later, a few studies concentrated on $\gamma$ transitions between molecular resonances in the $^{12}\mathrm{C} + ^{12}\mathrm{C}$ [12] and $\alpha + \alpha$ [13] collisions as a test of cluster structures. However, the relative lack of experimental interest for light-ion bremsstrahlung recently started to be reversed with the perspective of using the $t(d, n\gamma)\alpha$ bremsstrahlung to diagnose plasmas in fusion experiments [14].

Let us briefly summarize different types of models that are, or will be, applied to the description of bremsstrahlung processes. In the microscopic cluster model, the internal wave functions of the colliding nuclei have a simple cluster structure in the harmonic-oscillator shell model and the scattering wave functions are fully antisymmetrized. The results are derived from an effective nucleon-nucleon interaction without fitted parameters. The potential model is also based on a cluster assumption but the clusters are treated as pointlike particles interacting with an effective nucleus-nucleus interaction. The cluster assumption is relaxed in *ab initio* models where the internal structures of the colliding nuclei are derived by solving multinucleon Schrödinger equations with a realistic nucleon-nucleon interaction, and the collision is described by fully antisymmetrized wave functions with the same interaction.

As shown in Ref. [15] for the $\alpha(\alpha, \alpha\gamma)\alpha$ bremsstrahlung, potential-model results are very sensitive to the potential used and do not agree well with a microscopic cluster model taking antisymmetrization exactly into account. The study of the much more complicated $t(d, n\gamma)\alpha$ bremsstrahlung at low energies will require using realistic forces in an *ab initio* description. *Ab initio* wave functions have recently been derived for this reaction [16]. It is crucial to prepare a study of $t(d, n\gamma)\alpha$ by improving and simplifying bremsstrahlung calculations within fully antisymmetrized models.

For the sake of completeness, let us notice that bremsstrahlung photons are observed in nuclear collisions involving heavier nuclei and in higher ranges of energies (see references in Refs. [17–20]). These processes cannot at present be studied in microscopic models but the description with phenomenological nucleon-nucleus or nucleus-nucleus potentials can give satisfactory results [18–20]. These potential models are essentially equivalent to the model derived by our group where special attention has been devoted to solving slow convergence problems [21]. Bremsstrahlung photons also provide useful information in other nuclear processes such as proton decay, $\alpha$ decay, fission, ... (see references in Refs. [19,20]). These processes can still be considered as continuum to continuum transitions since the initial decaying state is not square-integrable. The photons are then emitted from the energy of the relative motion of the final particles. These processes can also be studied in variants of the potential model.

From now on, we focus on the microscopic description of bremsstrahlung at low energies. Early theoretical studies were based on an expansion in powers of the photon energy where the coefficients only depend on the on-shell scattering amplitudes [22]. A significant progress came with a microscopic model of the $\alpha(\alpha, \alpha\gamma)\alpha$ bremsstrahlung [23] using an effective nucleon-nucleon (NN) interaction within the framework of the resonating-group method (RGM). A good agreement with the few experimental data was obtained. This opened the way to studies of various bremsstrahlung reactions between light ions within the RGM [24–26] and

*jdoheter@ulb.ac.be
†dbaye@ulb.ac.be

 

within a potential model [27]. The calculation of cross sections suffered from a slowness of convergence due to the Coulomb part of the interaction. This problem was solved for both potential and microscopic models by a separate treatment of the Coulomb terms, which can be summed up exactly [21]. Microscopic studies then focused on evaluations of the model dependence of the calculations [15,28] and extensions to heavier systems [29,30]. A particularity of those calculations of bremsstrahlung cross sections is that the so-called Siegert theorem, i.e. the replacement of the current form of the electric transition operators by the charge-density form, could not be applied because of divergences in some matrix elements.

Describing electromagnetic transitions in nuclear systems requires a fair knowledge of the nuclear current. This current depends on the motion of the nucleons but also on the motion of the mesons which are responsible for the NN interaction. The contribution of the meson exchange currents is not fully known and their inclusion in the nuclear models is a heavy work. This problem was not addressed in previous nucleus-nucleus bremsstrahlung studies [15,21,23–30] where the meson exchange currents were neglected. At low photon energies, when the long-wavelength approximation can be applied, the direct inclusion of the meson exchange currents is needlessly complicated because the electric transitions can be described from the charge density rather than from the current density. Since the effects of the nuclear interaction on the charge density are weak, as first noted by Siegert [31], they can be neglected to a good approximation. However, the long-wavelength approximation cannot be performed in the bremsstrahlung calculations because it leads to mathematical divergences. The dependence of the bremsstrahlung description on the nuclear current cannot be fully removed. We propose to reduce it nevertheless greatly by using an extension of the Siegert theorem valid for arbitrary photon energy [32].

Based on the extended Siegert theorem, a microscopic cluster model of bremsstrahlung is developed and applied to the $\alpha + \alpha$ system for which experimental data are available. The $\alpha(\alpha, \alpha\gamma)\alpha$ bremsstrahlung reaction allows an evaluation of the importance of corrections due to meson exchange currents. Moreover, it allows testing the molecular structure of $^8$Be by a comparison of on-resonance $4^+ \rightarrow 2^+$ cross sections with off-resonance data [13]. The present study should open the way to *ab initio* studies of bremsstrahlung and in particular of the $t(d, n\gamma)\alpha$ bremsstrahlung based on recent *ab initio* wave functions of the $t(d, n)\alpha$ transfer reaction [16].

In Sec. II, the photon-emission operator is defined and its Siegert form is derived. Then, the microscopic cluster model of bremsstrahlung is described and the calculations of the electric transition matrix elements are explained. In Sec. III, the model is applied to the $\alpha + \alpha$ system for an effective NN interaction adapted to the cluster approach. The cross sections obtained with this Siegert approach are compared with the non-Siegert cross sections and with experimental data. The effects of the nuclear current in the Siegert approach are also analyzed. Concluding remarks are presented in Sec. IV.

## II. NUCLEUS-NUCLEUS BREMSSTRAHLUNG MODEL

### A. Cross sections

Two nuclei with reduced mass $\mu$ collide at the initial relative momentum $\boldsymbol{p}_i = \hbar \boldsymbol{k}_i$ in the $z$ direction and energy $E_i = p_i^2/2\mu$. After emission of a photon with energy $E_\gamma$ and momentum $\boldsymbol{p}_\gamma = \hbar \boldsymbol{k}_\gamma$ in the direction $\Omega_\gamma = (\theta_\gamma, \varphi_\gamma)$, the system has a final momentum $\boldsymbol{p}_f = \hbar \boldsymbol{k}_f$ in the direction $\Omega_f = (\theta_f, \varphi_f)$ and an energy $E_f = p_f^2/2\mu$, which satisfies

$$E_f = E_i - E_\gamma, \tag{1}$$

where the small recoil energy is neglected. For the sake of clarity, the presentation is restricted to spinless nuclei. Moreover, the nuclei are assumed to be the same in the initial and final states.

Evaluating the bremsstrahlung cross sections requires calculating the matrix element of the photon-emission operator $H_e$ between the incoming initial state $\Psi_i^{(+)}$ with energy $E_i$ and the outgoing final state $\Psi_f^{(-)}(\Omega_f)$ with energy $E_f$ and direction $\Omega_f$.

The photon-emission operator $H_e$ can be expanded as a sum of multipoles [33],

$$H_e = -\sum_{\lambda\mu\sigma} q^\sigma (-1)^\lambda \alpha_\lambda^\sigma \mathcal{M}_{\lambda\mu}^\sigma \mathcal{D}_{\mu-q}^\lambda (-\varphi_\gamma, -\theta_\gamma, 0), \tag{2}$$

where $q = \pm 1$ is the circular polarization, $\mathcal{D}_{\mu-q}^\lambda$ is the rotation matrix depending on the Euler angles $(-\varphi_\gamma, -\theta_\gamma, 0)$, $\mathcal{M}_{\lambda\mu}^\sigma$ is an electromagnetic transition multipole operator, $\sigma = 0$ or E corresponds to an electric multipole and $\sigma = 1$ or M corresponds to a magnetic multipole, and $\alpha_\lambda^\sigma$ is given by

$$\alpha_\lambda^\sigma = -\frac{\sqrt{2\pi(\lambda+1)}\, i^{\lambda+\sigma} k_\gamma^\lambda}{\sqrt{\lambda(2\lambda+1)}(2\lambda-1)!!}. \tag{3}$$

Defining the multipole matrix elements by

$$u_{\lambda\mu}^\sigma(\Omega_f) = \alpha_\lambda^\sigma \langle \Psi_f^{(-)}(\Omega_f) | \mathcal{M}_{\lambda\mu}^\sigma | \Psi_i^{(+)} \rangle, \tag{4}$$

the differential bremsstrahlung cross section is given by [21]

$$\frac{d\sigma}{dE_\gamma} = \frac{E_\gamma}{\pi^2 \hbar^5 c} \frac{p_f^2}{1+\delta_{12}} \times \sum_{\sigma\lambda\mu} \int_0^\pi (2\lambda+1)^{-1} \left| u_{\lambda\mu}^\sigma(\theta_f, 0) \right|^2 \sin\theta_f d\theta_f, \tag{5}$$

where $\delta_{12}$ is equal to unity if nuclei 1 and 2 are identical and to zero otherwise. This formula is not specific to the microscopic approach but is also valid in the potential model for instance [21]. The explicit formulas to obtain other differential bremsstrahlung cross sections from the multipole matrix element $u_{\lambda\mu}^\sigma$ can be found in Refs. [21,23]. They are not repeated here.

To calculate the matrix element $u_{\lambda\mu}^\sigma$, the initial and final states are expanded in partial waves. In a numerical approach, for some configurations, many partial waves are required to reach convergence. However, nuclear effects are restricted to few partial waves whereas Coulomb effects contribute up to much higher orbital momenta. As explained in Ref. [21], the bremsstrahlung matrix element can be separated into a

purely Coulomb part and a fast-converging series. Then, $u^{\sigma}_{\lambda\mu}$ can be approximated by

$$u^{\sigma}_{\lambda\mu} \approx u^{\sigma\mathrm{C}}_{\lambda\mu}[\infty] + u^{\sigma}_{\lambda\mu}[l_{\max}] - u^{\sigma\mathrm{C}}_{\lambda\mu}[l_{\max}], \tag{6}$$

where $u^{\sigma}_{\lambda\mu}[l_{\max}]$ means that only the partial waves up to the orbital momentum $l_{\max}$ are taken into account in the calculation of $u^{\sigma}_{\lambda\mu}$. The index C is added when the matrix element is calculated in a purely Coulombic pointlike nuclei approach. The truncated series $u^{\sigma}_{\lambda\mu}[l_{\max}] - u^{\sigma\mathrm{C}}_{\lambda\mu}[l_{\max}]$ converges for small values of $l_{\max}$ since the nuclear effects are restricted to few partial waves. In the Coulomb contribution $u^{\sigma\mathrm{C}}_{\lambda\mu}[\infty]$, the partial wave expansion is summed up analytically, thus avoiding the problem of the slow convergence [21].

### B. Electric multipole operators

Since only the electric transitions are concerned by the Siegert approach and since they dominate for light-ion bremsstrahlung at low photon energy, the magnetic transitions are not considered hereafter. The electric transition multipole operators are defined by [34]

$$\mathcal{M}^{\mathrm{E}}_{\lambda\mu} = \sqrt{\frac{\lambda}{\lambda+1}}\frac{(2\lambda+1)!!}{k_\gamma^\lambda c}\int \boldsymbol{J}\cdot\boldsymbol{A}^{\mathrm{E}}_{\lambda\mu}d\boldsymbol{r}, \tag{7}$$

where $\boldsymbol{J}$ is the intrinsic nuclear current density and $\boldsymbol{A}^{\mathrm{E}}_{\lambda\mu}$ is the electric multipole defined, in the Coulomb gauge, as [35]

$$\boldsymbol{A}^{\mathrm{E}}_{\lambda\mu}(\boldsymbol{r}) = \frac{i}{k_\gamma\sqrt{\lambda(\lambda+1)}}\boldsymbol{\chi}_{\lambda\mu}(k_\gamma,\boldsymbol{r}) \tag{8}$$

with

$$\boldsymbol{\chi}_{\lambda\mu}(k,\boldsymbol{r}) = \left(k_\gamma^2\boldsymbol{r} + \boldsymbol{\nabla}\frac{\partial}{\partial r}r\right)\phi_{\lambda\mu}(k_\gamma\boldsymbol{r}), \tag{9}$$

$$\phi_{\lambda\mu}(k\boldsymbol{r}) = j_\lambda(kr)Y_{\lambda\mu}(\Omega), \tag{10}$$

and $\boldsymbol{r} = (r,\Omega)$.

The current density $\boldsymbol{J}$ can be divided in two parts [36],

$$\boldsymbol{J} = \boldsymbol{J}_c + \boldsymbol{J}_m, \tag{11}$$

where $\boldsymbol{J}_c$ is associated with the charge density and $\boldsymbol{J}_m$ with the magnetization density. The current $\boldsymbol{J}_c$ depends not only on the motion of the protons but also on the motion of charged mesons or non-nucleonic constituents, therefore on the NN interaction too. However, evaluating the meson currents and taking directly their effects into account is a heavy task, all the heavier as the nuclear interaction is complicated. At low photon energy, a common method to get around this difficulty is to deduce the electric transition multipoles from the charge density rather than from the current density. The effects of the nuclear interaction on the charge density being weak, they can be neglected to a good approximation [31]. However, the full removal of the current density in the expression of the electric transition multipole is only possible at the long-wavelength approximation, which cannot be performed in the bremsstrahlung calculations. Indeed, since the initial and final states are in the continuum and hence not square-integrable, the long-wavelength approximation leads to divergent matrix elements of the electric transition multipole operators. Nevertheless, the current-density dependence of the electric transition multipole operator can be largely reduced by using an extension of the Siegert theorem for arbitrary photon energy [32]. Let us summarize this approach.

The electric multipole $\boldsymbol{A}^{\mathrm{E}}_{\lambda\mu}$ is divided into a gradient term and a rest,

$$\boldsymbol{A}^{\mathrm{E}}_{\lambda\mu}(\boldsymbol{r}) = \boldsymbol{\nabla}\Phi_{\lambda\mu}(\boldsymbol{r}) + \boldsymbol{A}'^{\mathrm{E}}_{\lambda\mu}(\boldsymbol{r}). \tag{12}$$

This separation is not unique since $\Phi_{\lambda\mu}$ can be chosen arbitrarily insofar as $\boldsymbol{A}'^{\mathrm{E}}_{\lambda\mu}$ is defined consistently. However, the compatibility with the Siegert theorem restricts to functions $\Phi_{\lambda\mu}$ with the behavior

$$\Phi_{\lambda\mu}(\boldsymbol{r}) \underset{k_\gamma\to 0}{\longrightarrow} \frac{i\sqrt{\lambda+1}k_\gamma^{\lambda-1}}{\sqrt{\lambda}(2\lambda+1)!!}\,r^\lambda Y_{\lambda\mu}(\Omega) \tag{13}$$

at low photon energies. Moreover, to avoid divergence problems, additional constraints on $\Phi_{\lambda\mu}$ are added,

$$r\Phi_{\lambda\mu}(\boldsymbol{r}) \text{ bounded}, \quad \frac{\partial}{\partial r}\Phi_{\lambda\mu}(\boldsymbol{r}) \underset{r\to\infty}{\longrightarrow} 0. \tag{14}$$

A practical choice of $\Phi_{\lambda\mu}$ is specified in Eq. (21). By inserting Eq. (12) in Eq. (7) and after an integration by parts, the divergence of the current density appears in the expression of $\mathcal{M}^{\mathrm{E}}_{\lambda\mu}$. It can then be removed by using the current conservation

$$\boldsymbol{\nabla}\cdot\boldsymbol{J}(\boldsymbol{r}) + \frac{i}{\hbar}[H,\rho(\boldsymbol{r})] = 0, \tag{15}$$

where $H$ is the internal Hamiltonian, i.e. with the center of mass (c.m.) removed, and $\rho$ is the internal charge density of the system of $A$ nucleons. Then, the electric transition multipole operator is written as

$$\mathcal{M}^{\mathrm{E}}_{\lambda\mu} = \sqrt{\frac{\lambda}{\lambda+1}}\frac{(2\lambda+1)!!}{k_\gamma^\lambda c} \times \int\left\{\frac{i}{\hbar}[H,\rho(\boldsymbol{r})]\Phi_{\lambda\mu}(\boldsymbol{r}) + \boldsymbol{J}\cdot\boldsymbol{A}'^{\mathrm{E}}_{\lambda\mu}\right\}d\boldsymbol{r}. \tag{16}$$

If $\Psi_i^{(+)}$ and $\Psi_f^{(-)}$ are assumed to be exact eigenstates of the internal Hamiltonian, the matrix element of the electric transition multipole operator between initial and final states is given by

$$\langle\Psi_f^{(-)}|\mathcal{M}^{\mathrm{E}}_{\lambda\mu}|\Psi_i^{(+)}\rangle = \sqrt{\frac{\lambda}{\lambda+1}}\frac{(2\lambda+1)!!}{k_\gamma^\lambda c} \times \int\langle\Psi_f^{(-)}|-ick_\gamma\rho(\boldsymbol{r})\Phi_{\lambda\mu}(\boldsymbol{r}) + \boldsymbol{J}\cdot\boldsymbol{A}'^{\mathrm{E}}_{\lambda\mu}|\Psi_i^{(+)}\rangle d\boldsymbol{r}, \tag{17}$$

where Eq. (1) is used. The r.h.s. of Eq. (17) defines the Siegert form of the electric transition multipole operator, noted as $\mathcal{M}^{\mathrm{E(S)}}_{\lambda\mu}$,

$$\mathcal{M}^{\mathrm{E(S)}}_{\lambda\mu} = \sqrt{\frac{\lambda}{\lambda+1}}\frac{(2\lambda+1)!!}{k_\gamma^\lambda c} \times \int\left[-ick_\gamma\rho(\boldsymbol{r})\Phi_{\lambda\mu}(\boldsymbol{r}) + \boldsymbol{J}\cdot\boldsymbol{A}'^{\mathrm{E}}_{\lambda\mu}\right]d\boldsymbol{r}. \tag{18}$$

As expected, at low photon energy, the dominant part of $\mathcal{M}^{\mathrm{E(S)}}_{\lambda\mu}$ only depends on the charge density and not on the

current density. Consequently, at low photon energy, using an approximate current should be more accurate in the Siegert operator (18) than in the non-Siegert operator (7).

To evaluate the residual contribution of the current density to the Siegert operator, an approximate Siegert operator fully neglecting the current is also defined as

$$\mathcal{M}^{\mathrm{E}(J=0)}_{\lambda\mu} = -i\sqrt{\frac{\lambda}{\lambda+1}}\frac{(2\lambda+1)!!}{k_\gamma^{\lambda-1}}\int \rho(\boldsymbol{r})\Phi_{\lambda\mu}(\boldsymbol{r})d\boldsymbol{r}. \quad (19)$$

Comparing the results obtained from $\mathcal{M}^{\mathrm{E(S)}}_{\lambda\mu}$ and $\mathcal{M}^{\mathrm{E}(J=0)}_{\lambda\mu}$ enables us to study the importance of the current-dependent term of the Siegert operator.

To define the Siegert operator in an unequivocal way, $\Phi_{\lambda\mu}$ has to be chosen. By inspection of Eq. (8), a natural choice seems to be

$$\Phi_{\lambda\mu}(\boldsymbol{r}) = \frac{i}{k_\gamma\sqrt{\lambda(\lambda+1)}}\frac{\partial}{\partial r}r\phi_{\lambda\mu}(k_\gamma\boldsymbol{r}). \quad (20)$$

However, this choice does not fulfill conditions (14). Other choices for $\Phi_{\lambda\mu}$ were considered in Ref. [32]. Among them, only the so-called standard choice fulfills Eq. (14) and enables us to have only convergent integrals in the calculation of matrix elements for electric transitions between two continuum states. This standard choice, which is considered hereafter in this paper, is defined by

$$\Phi_{\lambda\mu}(\boldsymbol{r}) = \frac{i\sqrt{\lambda+1}}{k_\gamma\sqrt{\lambda}}\phi_{\lambda\mu}(k_\gamma\boldsymbol{r}). \quad (21)$$

In a conceptual point of view, the arbitrary nature of this choice is not problematic since it has, in principle, no influence. The Siegert and non-Siegert operators, defined by Eqs. (18) and (7), lead exactly to the same results if consistent current and charge densities are considered and the exact eigenstates of the internal Hamiltonian are used. However, in many-body nuclear models, the eigenstates of the Hamiltonian as well as the current and charge densities are known only approximately. In practice, differences between the Siegert and non-Siegert approaches can thus arise and the particular choice of $\Phi_{\lambda\mu}$ could have some effects on the results. Nevertheless, at low photon energy, these effects are weak as will be explained in Sec. II D. Differences between the Siegert and non-Siegert approaches are studied in Sec. III for the $\alpha+\alpha$ system.

Let us specify the current and charge densities that are considered here. To limit the complexity of the calculations, the current density for free nucleons is considered. In this approximation, regarding the nucleons as point particles with a charge and a magnetic moment, the charge current density is given by [34]

$$\boldsymbol{J}_c(\boldsymbol{r}) = \frac{e}{2m_N}\sum_{j=1}^{A}\left(\frac{1}{2}-t_{j3}\right) \times [\boldsymbol{p}_j - A^{-1}\boldsymbol{P}_{\mathrm{c.m.}}, \delta(\boldsymbol{r}_j - \boldsymbol{R}_{\mathrm{c.m.}} - \boldsymbol{r})]_+, \quad (22)$$

where $[\boldsymbol{a},\boldsymbol{b}]_+$ is a shorthand notation for $\boldsymbol{a}\cdot\boldsymbol{b}+\boldsymbol{b}\cdot\boldsymbol{a}$, the magnetization current density by

$$\boldsymbol{J}_m(\boldsymbol{r}) = \frac{e}{2m_N}\sum_{j=1}^{A} g_{sj}\nabla\times\delta(\boldsymbol{r}_j - \boldsymbol{R}_{\mathrm{c.m.}} - \boldsymbol{r})\boldsymbol{s}_j, \quad (23)$$

and the charge density by

$$\rho(\boldsymbol{r}) = e\sum_{j=1}^{A}\left(\frac{1}{2}-t_{j3}\right)\delta(\boldsymbol{r}_j - \boldsymbol{R}_{\mathrm{c.m.}} - \boldsymbol{r}). \quad (24)$$

In these expressions, $A$ is the mass number of the system, $m_N$ is the nucleon mass, $\boldsymbol{r}_j$, $\boldsymbol{p}_j$, $\boldsymbol{s}_j$, and $\boldsymbol{t}_j$ are the coordinate, momentum, spin, and isospin of nucleon $j$, $\boldsymbol{R}_{\mathrm{c.m.}}$ and $\boldsymbol{P}_{\mathrm{c.m.}}$ are the c.m. coordinate and momentum, and $g_{sj} = (g_n+g_p)/2 + t_{j3}(g_n-g_p)$ where $g_n$ and $g_p$ are the neutron and proton gyromagnetic factors, respectively.

From these current densities, the non-Siegert electric transition multipole operators are given explicitly by [37]

$$\mathcal{M}^{\mathrm{E}}_{\lambda\mu} = \frac{ie(2\lambda+1)!!}{m_N c(\lambda+1)k_\gamma^{\lambda+1}} \times\sum_{j=1}^{A}\left[\left(\frac{1}{2}-t_{j3}\right)\boldsymbol{\chi}_{\lambda\mu}(k_\gamma,\boldsymbol{r})\cdot(\boldsymbol{p}_j - A^{-1}\boldsymbol{P}_{\mathrm{c.m.}}) - \frac{1}{2}k_\gamma^2 g_{sj}(\boldsymbol{r}\times\nabla)\phi_{\lambda\mu}(k_\gamma\boldsymbol{r})\cdot\boldsymbol{s}_j\right]_{\boldsymbol{r}=\boldsymbol{r}_j-\boldsymbol{R}_{\mathrm{c.m.}}}. \quad (25)$$

This is the expression used in earlier works. The spin-independent part of $\mathcal{M}^{\mathrm{E}}_{\lambda\mu}$ comes from the convection current density $\boldsymbol{J}_c$ and the spin-dependent part from the magnetization current density $\boldsymbol{J}_m$. The Siegert electric transition multipole operators are written explicitly with Eq. (21) as

$$\mathcal{M}^{\mathrm{E(S)}}_{\lambda\mu} = \frac{e(2\lambda+1)!!}{k_\gamma^\lambda}\sum_{j=1}^{A}\left(\frac{1}{2}-t_{j3}\right)\phi_{\lambda\mu}[k_\gamma(\boldsymbol{r}_j - \boldsymbol{R}_{\mathrm{c.m.}})] + \frac{ie(2\lambda+1)!!}{2m_N c(\lambda+1)k_\gamma^{\lambda+1}}\sum_{j=1}^{A}\left\{\left(\frac{1}{2}-t_{j3}\right)[\boldsymbol{\chi}_{\lambda\mu}(k_\gamma,\boldsymbol{r}) - (\lambda+1)\nabla\phi_{\lambda\mu}(k_\gamma\boldsymbol{r}), \boldsymbol{p}_j - A^{-1}\boldsymbol{P}_{\mathrm{c.m.}}]_+ - k_\gamma^2 g_{sj}(\boldsymbol{r}\times\nabla)\phi_{\lambda\mu}(k_\gamma\boldsymbol{r})\cdot\boldsymbol{s}_j\right\}_{\boldsymbol{r}=\boldsymbol{r}_j-\boldsymbol{R}_{\mathrm{c.m.}}}. \quad (26)$$

The first sum in Eq. (26) comes from the charge density. The second sum comes from the current density (the spin-independent part from $\boldsymbol{J}_c$ and the spin-dependent part from $\boldsymbol{J}_m$). At the approximation where the current is neglected, the Siegert operator is thus limited to the first sum,

$$\mathcal{M}^{\mathrm{E}(J=0)}_{\lambda\mu} = \frac{e(2\lambda+1)!!}{k_\gamma^\lambda}\sum_{j=1}^{A}\left(\frac{1}{2}-t_{j3}\right)\phi_{\lambda\mu}[k_\gamma(\boldsymbol{r}_j - \boldsymbol{R}_{\mathrm{c.m.}})]. \quad (27)$$

The spin term is the same for the Siegert and non-Siegert operators since

$$\int \boldsymbol{J}_m\cdot\boldsymbol{A}'^{\mathrm{E}}_{\lambda\mu}d\boldsymbol{r} = \int \boldsymbol{J}_m\cdot\boldsymbol{A}^{\mathrm{E}}_{\lambda\mu}d\boldsymbol{r}. \quad (28)$$

As the effects of the nuclear interaction are expected to be weaker on the charge density than on the current density [31], the Siegert operator $\mathcal{M}^{\mathrm{E(S)}}_{\lambda\mu}$ should have preference over $\mathcal{M}^{\mathrm{E}}_{\lambda\mu}$.

### C. Scattering wave functions

The scattering wave functions are described by the same model as in Ref. [23]. Their definition is briefly summarized here.

In the microscopic cluster approaches, the scattering wave functions can be expanded in partial waves defined by

$$\psi^{lm} = \sqrt{\frac{A!}{A_1!A_2!(1+\delta_{12})}}\mathcal{A}\phi_1\phi_2 Y_l^m(\Omega_\rho)g^l(\rho), \qquad (29)$$

where $A_1$ and $A_2$ are the mass numbers of nuclei 1 and 2, $\mathcal{A}$ is the antisymmetrization projector, $\boldsymbol{\rho} = (\rho, \Omega_\rho)$ is the relative coordinate between the cluster c.m., and $\phi_1$ and $\phi_2$ are the internal wave functions of nuclei 1 and 2. To simplify the presentation, the spins of the colliding nuclei are not considered here and hereafter.

In the generator coordinate method (GCM) version of the model [38,39], a particular ansatz is considered for $\phi_1$ and $\phi_2$, allowing a systematic calculation of the matrix elements. The internal wave functions $\phi_1$ and $\phi_2$ are obtained by removing a c.m. factor from Slater determinants describing the ground states of the clusters within the harmonic oscillator shell model. The same oscillator parameter $b$ is used for both nuclei. The $g^l$ relative function is approximated as a sum of projected Gaussian functions $\Gamma_l(\rho, R_n)$ defined by

$$\Gamma_l(\rho, R_n) = (\mu'/\pi b^2)^{3/4} e^{-\mu'(\rho^2+R_n^2)/2b^2} i_l(\mu'\rho R_n/b^2), \qquad (30)$$

where $R_n$ are real parameters called generator coordinates, $\mu' = \mu/m_N$, and $i_l$ is a modified spherical Bessel function of the first kind or spherical Hankel function. This particular choice of $g^l$ enables us to rewrite $\psi^{lm}$ as a function of Slater determinants,

$$\phi_{\text{c.m.}}\psi^{lm} = \sum_n f_n^l \phi^{lm}(R_n), \qquad (31)$$

where $\phi_{\text{c.m.}} \propto \exp(-AR_{\text{c.m.}}^2/2b^2)$ is the c.m. harmonic-oscillator $0s$ wave function with the oscillator parameter $b/\sqrt{A}$ centered around the origin. The function $\phi^{lm}(R_n)$ is the projection on the relative orbital momentum $l$ of a Slater determinant in the two-center harmonic-oscillator shell model with centers separated by a distance $R_n$. The key point of the GCM is that the matrix elements between Slater determinants can be evaluated efficiently and systematically. The main drawback of the GCM expansion (31) is that the projected Gaussian functions are not able to reproduce the correct asymptotic behavior of the relative function $g^l$. This problem is solved by the microscopic $R$-matrix method (MRM) [40,41]. In this approach, the configuration space is divided at the channel radius $a$ into two regions: an internal region where $\rho < a$ and an external region where $\rho > a$. In the internal region, the scattering wave function is described by the GCM as explained before with full account of the antisymmetrization. In the external region, the antisymmetrization between the colliding nuclei is neglected and the radial relative function $g^l$ is approximated by its asymptotic behavior,

$$\psi_{\text{ext}}^{lm} = \phi_1\phi_2 Y_l^m(\Omega_\rho) g_{\text{ext}}^l(\rho) \qquad (32)$$

with

$$g_{\text{ext}}^l(\rho) = 2[\pi(1+\delta_{12})(2l+1)/v]^{1/2} i^l e^{i(\sigma_l+\delta_l)} \times [F_l(\eta, k\rho)\cos\delta_l + G_l(\eta, k\rho)\sin\delta_l]/k\rho, \qquad (33)$$

where $F_l$ and $G_l$ are the regular and irregular Coulomb functions, $\eta$ is the Sommerfeld parameter, $\sigma_l$ and $\delta_l$ are the Coulomb and nuclear phase shifts, and $k$ and $v$ are the relative wave number and velocity. When the colliding nuclei are identical, a residual effect of the antisymmetrization between the nuclei in the external region is that Eq. (32) must be properly symmetrized. The partial wave expansion has to be limited to even values of $l$ if the colliding nuclei are identical bosons.

The coefficients $f_n^l$ of Eq. (31) and the nuclear phase shifts $\delta_l$ are evaluated by solving a Bloch-Schrödinger equation based on a microscopic Hamiltonian, associated with the continuity condition between $\psi_{\text{int}}^{lm}$ and $\psi_{\text{ext}}^{lm}$ at $a$ [40,41]. The wave function is insensitive to the value of $a$ if $a$ is chosen large enough, i.e., larger than the range of the nuclear forces and of antisymmetrization effects between nucleons belonging to different nuclei.

### D. Matrix elements of electric transition multipole operators

The calculation of the matrix elements of the electric transition multipole operators $\mathcal{M}_{\lambda\mu}^{\text{E}}$ between partial waves was previously discussed in Ref. [23], but the calculation for the Siegert operator $\mathcal{M}_{\lambda\mu}^{\text{E(S)}}$ is new. For the sake of comparison, the calculations for both operators are detailed here.

Let us note $\mathcal{M}_{\lambda\mu}$ for $\mathcal{M}_{\lambda\mu}^{\text{E}}$, $\mathcal{M}_{\lambda\mu}^{\text{E(S)}}$, or $\mathcal{M}_{\lambda\mu}^{\text{E}(J=0)}$. The matrix element of $\mathcal{M}_{\lambda\mu}$ is approximated with a good accuracy by [23]

$$\langle\psi^{l_f m_f}|\mathcal{M}_{\lambda\mu}|\psi^{l_i m_i}\rangle = \langle\psi_{\text{int}}^{l_f m_f}|\widetilde{\mathcal{M}}_{\lambda\mu}|\psi_{\text{int}}^{l_i m_i}\rangle - \langle\psi_{\text{int}}^{l_f m_f}|\widetilde{\mathcal{M}}_{\lambda\mu}|\psi_{\text{int}}^{l_i m_i}\rangle_{\text{ext}} + \langle\psi_{\text{ext}}^{l_f m_f}|\mathcal{M}_{\lambda\mu}|\psi_{\text{ext}}^{l_i m_i}\rangle_{\text{ext}}, \qquad (34)$$

where the first matrix element is calculated microscopically over the whole space while the last two are evaluated over the external region, by neglecting the antisymmetrization. The operator $\widetilde{\mathcal{M}}_{\lambda\mu}$ is the long-wavelength approximation of $\mathcal{M}_{\lambda\mu}$. Replacing $\mathcal{M}_{\lambda\mu}$ by $\widetilde{\mathcal{M}}_{\lambda\mu}$ can be done for the matrix elements between $\psi_{\text{int}}^{l_i m_i}$ and $\psi_{\text{int}}^{l_f m_f}$ without that convergence problems arise since the wave functions in the internal region are square-integrable. This substitution is not essential but it leads to much less complicated matrix elements.

At the long-wavelength approximation, the Siegert operator $\widetilde{\mathcal{M}}_{\lambda\mu}^{\text{E(S)}}$ is deduced from Eq. (13). Performing the long-wavelength approximation enables thus one to eliminate totally the dependence on the current and on the particular choice of $\Phi_{\lambda\mu}$ in the Siegert operator.

The electric transition multipole operators are explicitly given at the long-wavelength approximation by

$$\widetilde{\mathcal{M}}_{\lambda\mu}^{\text{E(S)}} = \widetilde{\mathcal{M}}_{\lambda\mu}^{\text{E}(J=0)} = e\sum_{j=1}^{A}\left(\frac{1}{2} - t_{j3}\right)\left[r^\lambda Y_\lambda^\mu(\Omega)\right]_{\boldsymbol{r}_j - \boldsymbol{R}_{\text{c.m.}}} \qquad (35)$$

and [23]

$$\widetilde{\mathcal{M}}^{\mathrm{E}}_{\lambda\mu} = \frac{ie}{m_N c k_\gamma} \sum_{j=1}^{A} \left(\frac{1}{2} - t_{j3}\right) \times \left[\nabla r^\lambda Y^\mu_\lambda(\Omega)\right]_{\boldsymbol{r}_j - \boldsymbol{R}_{\mathrm{c.m.}}} \cdot \left(\boldsymbol{p}_j - A^{-1}\boldsymbol{P}_{\mathrm{c.m.}}\right). \quad (36)$$

The Siegert operator $\widetilde{\mathcal{M}}^{\mathrm{E(S)}}_{\lambda\mu}$ has the advantage over the non-Siegert operator $\widetilde{\mathcal{M}}^{\mathrm{E}}_{\lambda\mu}$ in that it depends only on the nucleon coordinates and not on the nucleon momenta. The calculation of the $\widetilde{\mathcal{M}}^{\mathrm{E(S)}}_{\lambda\mu}$ matrix element is thus easier. Moreover, the initial and final states, which are considered in this model, are not exact. Since the wave functions are generally better known than their derivatives, it is preferable to avoid derivatives when it is possible, as recommended in Ref. [36].

The calculation of the first term of the r.h.s. of Eq. (34) is simplified by working with individual nucleon coordinates thanks to the property [23,42]

$$\left\langle \psi^{l_f m_f}_{\mathrm{int}} \middle| \widetilde{\mathcal{M}}_{\lambda\mu} \middle| \psi^{l_i m_i}_{\mathrm{int}} \right\rangle = \left\langle \phi_{\mathrm{c.m.}} \psi^{l_f m_f}_{\mathrm{int}} \middle| \widetilde{\mathcal{M}}_{\lambda\mu}(\mathrm{o.b.}) \middle| \phi_{\mathrm{c.m.}} \psi^{l_i m_i}_{\mathrm{int}} \right\rangle, \quad (37)$$

where $\widetilde{\mathcal{M}}_{\lambda\mu}(\mathrm{o.b.})$ is the one-body form of $\widetilde{\mathcal{M}}_{\lambda\mu}$ obtained by replacing $\boldsymbol{r}_j - \boldsymbol{R}_{\mathrm{c.m.}}$ by $\boldsymbol{r}_j$ and $\boldsymbol{p}_j - A^{-1}\boldsymbol{P}_{\mathrm{c.m.}}$ by $\boldsymbol{p}_j$. The r.h.s. of Eq. (37) is the matrix element of a one-body operator evaluated between linear combinations of projected Slater determinants. Therefore, it can be evaluated efficiently with Brink-Löwdin techniques [43,44]. Equation (37) comes from the particular form of the scattering wave function.

The calculation of the matrix elements evaluated over the external region in Eq. (34) is simplified by neglecting the antisymmetrization between nuclei, consistently with the $R$-matrix approach. Again, a symmetrization between nuclei has to be considered if colliding nuclei are identical, but it causes no additional difficulty. Over the external region, the asymptotic form of the electric transition multipole operators can be used. Then, the matrix elements over the external region can be expressed as one-dimensional integrals, as in Ref. [23]. The matrix element of $\mathcal{M}_{\lambda\mu}$ between the external parts of the wave functions is given by

$$\left\langle \psi^{l_f m_f}_{\mathrm{ext}} \middle| \mathcal{M}_{\lambda\mu} \middle| \psi^{l_i m_i}_{\mathrm{ext}} \right\rangle_{\mathrm{ext}} = (2\lambda+1)!! k_\gamma^{-\lambda-1} \frac{e\hbar}{\mu c} \int Y^{m_f *}_{l_f} Y^\mu_\lambda Y^{m_i}_{l_i} d\Omega_\rho \times \left[Z_1 \overline{\mathcal{M}}_\lambda(A_2 k_\gamma/A) + (-1)^\lambda Z_2 \overline{\mathcal{M}}_\lambda(A_1 k_\gamma/A)\right], \quad (38)$$

where $\overline{\mathcal{M}}_\lambda$ is given in the Siegert form by

$$\overline{\mathcal{M}}^{\mathrm{E(S)}}_\lambda(k) = \overline{\mathcal{M}}^{\mathrm{E}}_\lambda(k) + \frac{a^2}{2} j_\lambda(ka) \left[g^{l_f *}_{\mathrm{ext}} \frac{d g^{l_i}_{\mathrm{ext}}}{d\rho} - g^{l_i}_{\mathrm{ext}} \frac{d g^{l_f *}_{\mathrm{ext}}}{d\rho}\right]_{\rho=a} + \frac{a^2}{2} \left[g^{l_f *}_{\mathrm{ext}} g^{l_i}_{\mathrm{ext}} \frac{d j_\lambda(k\rho)}{d\rho}\right]_{\rho=a}, \quad (39)$$

or when the current term is neglected by

$$\overline{\mathcal{M}}^{\mathrm{E}(J=0)}_\lambda(k) = \frac{\mu c}{\hbar} k_\gamma \int_a^\infty \rho^2 g^{l_f *}_{\mathrm{ext}} g^{l_i}_{\mathrm{ext}} j_\lambda(k\rho) d\rho, \quad (40)$$

and in the non-Siegert form by [23]

$$\overline{\mathcal{M}}^{\mathrm{E}}_\lambda(k) = \frac{1}{2(\lambda+1)} [\lambda(\lambda+1) + l_i(l_i+1) - l_f(l_f+1)] \times \int_a^\infty g^{l_f *}_{\mathrm{ext}} g^{l_i}_{\mathrm{ext}} \frac{d}{d\rho} \rho j_\lambda(k\rho) d\rho + \lambda \int_a^\infty \rho g^{l_f *}_{\mathrm{ext}} \frac{d g^{l_i}_{\mathrm{ext}}}{d\rho} j_\lambda(k\rho) d\rho. \quad (41)$$

The Siegert and non-Siegert matrix elements over the external region only differ by a term evaluated at the channel radius. However, if the long-wavelength approximation is accurate over the internal region, it should remain accurate at the channel radius too. If the long-wavelength approximation is applied to the term evaluated at the channel radius, the Siegert matrix element over the external region no longer depends on the particular choice of $\Phi_{\lambda\mu}$, as is the case for the Siegert matrix element over the internal region. Consequently, at low photon energy, the Siegert matrix element is nearly insensitive to the particular choice of $\Phi_{\lambda\mu}$ when conditions (13) and (14) are satisfied.

The integrals appearing in Eqs. (40) and (41) converge very slowly, which makes a numerical integration tedious. However, the convergence rate can be greatly improved by using a contour integration method [45], widely applied in the continuum-to-continuum electromagnetic transition framework [23,24,46]. This method is detailed in the Appendix.

The second term of the r.h.s. of Eq. (34) is obtained from Eqs. (38)–(41) by replacing $g_{\mathrm{ext}}$ by $g_{\mathrm{int}}$ and $j_\lambda(k\rho)$ by $(k\rho)^\lambda/(2\lambda+1)!!$. Only the terms of the lowest order in $k\rho$ are kept, since for this matrix element the electric multipole is considered at the long-wavelength approximation. After simplifications, one obtains

$$\left\langle \psi^{l_f m_f}_{\mathrm{int}} \middle| \widetilde{\mathcal{M}}_{\lambda\mu} \middle| \psi^{l_i m_i}_{\mathrm{int}} \right\rangle_{\mathrm{ext}} = \frac{e\hbar}{\mu c k_\gamma A^\lambda} \left[Z_1 A_2^\lambda + (-1)^\lambda Z_2 A_1^\lambda\right] \widehat{\mathcal{M}}_\lambda \times \int Y^{m_f *}_{l_f} Y^\mu_\lambda Y^{m_i}_{l_i} d\Omega_\rho, \quad (42)$$

where $\widehat{\mathcal{M}}_\lambda$ is given by

$$\widehat{\mathcal{M}}^{\mathrm{E(S)}}_\lambda = \widehat{\mathcal{M}}^{\mathrm{E}(J=0)}_\lambda = \frac{\mu c}{\hbar} k_\gamma \int_a^\infty \rho^{\lambda+2} g^{l_f *}_{\mathrm{int}} g^{l_i}_{\mathrm{int}} d\rho \quad (43)$$

and

$$\widehat{\mathcal{M}}^{\mathrm{E}}_\lambda = \frac{1}{2} [\lambda(\lambda+1) + l_i(l_i+1) - l_f(l_f+1)] \times \int_a^\infty \rho^\lambda g^{l_f *}_{\mathrm{int}} g^{l_i}_{\mathrm{int}} d\rho + \lambda \int_a^\infty \rho^{\lambda+1} g^{l_f *}_{\mathrm{int}} \frac{d g^{l_i}_{\mathrm{int}}}{d\rho} d\rho. \quad (44)$$

## III. APPLICATION TO $\alpha + \alpha$ BREMSSTRAHLUNG

### A. Model specifications

The model developed here is applied to the $\alpha + \alpha$ bremsstrahlung, which is one of a few collisions between light

ions for which experimental data exist. The results obtained with the Siegert operator are compared with the ones obtained with the non-Siegert operator and with experimental data when they are available. The importance of the current-dependent term of the Siegert operator is evaluated by comparing results obtained with the full Siegert operator and with the Siegert operator with the current term neglected.

For the $\alpha + \alpha$ system, odd-parity multipoles are forbidden since the $\alpha$ particles are bosons and $M1$ transitions are forbidden at the long-wavelength approximation because of the orthogonality between the initial and final states [42]. Only the $E2$ dominant transitions are considered here. The oscillator parameter $b$ is set at 1.36 fm to reproduce the experimental $\alpha$ radius. Ten generator coordinates varying from 0.5 to 7.7 fm with a step of 0.8 fm are used to describe the wave function in the internal region. The effective NN interaction is the sum of the central part of the Minnesota interaction [47] and the Coulomb potential. The exchange parameter $u$ is set at the value 0.9474 to reproduce with this model the experimental phase shifts with a good accuracy [48]. The matrix elements $u^{\mathrm{E}}_{2\mu}$ are calculated by Eq. (6) with $l_{\max} = 8$. The results are not modified significantly when $l_{\max}$ is increased from 8 to 10. The purely Coulombic matrix element $u^{\sigma\mathrm{C}}_{\lambda\mu}[\infty]$ is calculated exactly following the method presented in Ref. [21]. This matrix element has the peculiarity of being exactly the same in the Siegert and non-Siegert approaches. Two values of the channel radius are considered in this model, $a = 5.3$ fm and $a = 6.1$ fm, to check the insensitivity of the results to the value of $a$. Only the results for $a = 5.3$ fm are displayed in the figures.

### B. Cross sections

In Fig. 1, the angle-integrated cross sections $d\sigma/dE_\gamma$ are shown for three values of the photon energy: $E_\gamma = 1$, 5, and 9 MeV. Relative differences between cross sections at the two considered values of the channel radius are smaller than 1% at $E_\gamma = 1$ MeV, 1.5% at 5 MeV, and 2.3% at 9 MeV. In all cases, the absolute differences are bounded by 0.5 nb/MeV. For all considered energies, differences between the Siegert approach and its null-current approximation are totally negligible. Differences between the Siegert and non-Siegert approaches are negligible at $E_\gamma = 1$ MeV too. They are still weak at $E_\gamma = 5$ MeV but they become quite important at $E_\gamma = 9$ MeV. These results indicate that the differences between the Siegert and non-Siegert approaches increase with the photon energy. This can be understood intuitively. Indeed, for a central NN interaction, the differences between the Siegert and non-Siegert approaches mainly come from the inaccuracy of the scattering wave functions, and hence from the cluster approximation. The lower the photon energy is, the weaker the contribution of the internal region to the bremsstrahlung matrix element is. Moreover, the larger the relative coordinate $\rho$ is, the more accurate the cluster approximation is. Hence, the results based on the Siegert and non-Siegert approaches must be close at low photon energy.

Let us compare the model results with experimental data. Only few experimental differential bremsstrahlung cross sections are available [10,11] and all of them are measured in the equal-angle coplanar Harvard geometry, for which the $\alpha$ particles are detected in the directions $\Omega_1 = (\theta, 0)$ and $\Omega_2 = (\theta, \pi)$. The photon is undetected. Differential bremsstrahlung cross sections for the Harvard configurations $\theta = 35^\circ$ and $\theta = 37^\circ$ are shown in Fig. 2.

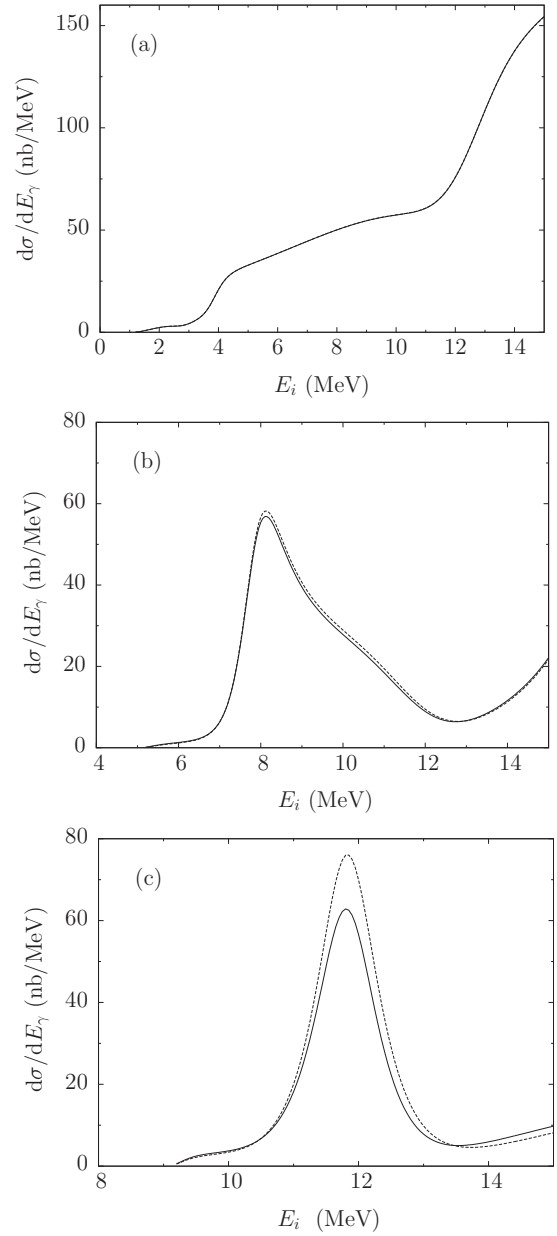


FIG. 1. Angle-integrated cross sections $d\sigma/dE_\gamma$ for $E_\gamma =$ (a) 1 MeV, (b) 5 MeV, and (c) 9 MeV as a function of the initial energy $E_i$. Full lines correspond to the Siegert operator $\mathcal{M}^{\mathrm{E(S)}}_{\lambda\mu}$ and dashed lines to the non-Siegert operator $\mathcal{M}^{\mathrm{E}}_{\lambda\mu}$. The null-current approximation $\mathcal{M}^{\mathrm{E}(J=0)}_{\lambda\mu}$ is indistinguishable from the full lines.

For the displayed energy ranges, absolute differences between cross sections at the two considered values of the channel radius are smaller than 0.08 $\mu$b/sr$^2$.

Again, differences between the Siegert approach and its null-current approximation are totally negligible. Since in the Harvard configuration the photon energy is proportional to the

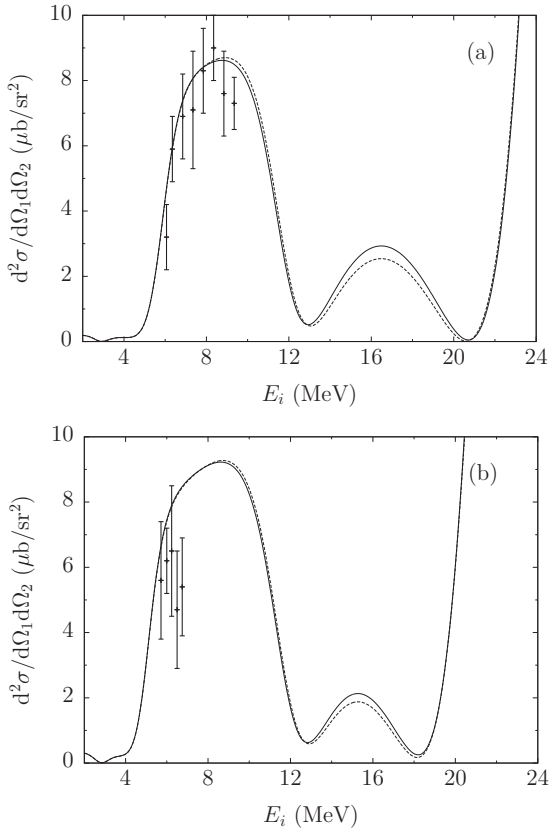


FIG. 2. Laboratory differential cross section $d^2\sigma/d\Omega_1 d\Omega_2$ in the coplanar geometry at (a) $\theta = 35^\circ$ and (b) $\theta = 37^\circ$ as a function of the initial energy $E_i$. Full lines correspond to the Siegert operator $\mathcal{M}^{\mathrm{E(S)}}_{\lambda\mu}$ and dashed lines to the non-Siegert operator $\mathcal{M}^{\mathrm{E}}_{\lambda\mu}$. The null-current approximation $\mathcal{M}^{\mathrm{E}(J=0)}_{\lambda\mu}$ is indistinguishable from the full lines. Experimental data are from Refs. [10,11].

initial energy, one notes again that the differences between the Siegert and non-Siegert approaches are weak at low photon energy. Experimental data being available only at low initial energy $E_i$, the photon energy given by

$$E_\gamma = (1 - \tan^2\theta)E_i \tag{45}$$

is rather small and the agreement with the experiments is similar for both approaches.

In a quite recent paper [13], cross sections of $\gamma$ transitions in $^8$Be were measured. They were interpreted as transitions from $4^+$ to $2^+$ states. However, since $^8$Be is unbound, radiative transitions in this nucleus are nothing but $\alpha + \alpha$ bremsstrahlung radiations and, though $4^+$ to $2^+$ transitions are dominant, radiative transitions take place actually between two continuum states. The bremsstrahlung model developed here enables a proper description of this experiment.

In Ref. [13], integrated cross sections are measured for two incident energies: one ($E_{\mathrm{res}}$) that should correspond to the $4^+$ resonance energy and the other ($E_{\mathrm{off}}$) that is above this resonance. Taking account of the energy loss of the beam in the intervening material before the collision, the on-resonance and off-resonance energies are given by $E_{\mathrm{res}} = 10.85$ MeV and $E_{\mathrm{off}} = 12.95$ MeV [49].

TABLE I. Theoretical and experimental cross sections $\sigma(E_{\mathrm{min}}, E_{\mathrm{max}})$ at $E_i = E_{\mathrm{res}}$ and $E_i = E_{\mathrm{off}}$. In parentheses, cross sections considering only $4^+$ to $2^+$ transitions are given. Experimental data come from Ref. [13].

| $E_i$ (MeV) | $E_{\mathrm{min}}$ (MeV) | $E_{\mathrm{max}}$ (MeV) | Siegert | Non-Siegert | Expt. |
|---|---|---|---|---|---|
| 10.85 | 5.0 | 12.5 | 200 (178) | 219 (199) | $165 \pm 54$ |
| 12.95 | 7.0 | 14.5 | 44 (12) | 53 (24) | $39 \pm 26$ |

The bremsstrahlung events are detected only if the photon energy is in a certain range. The integrated cross sections that are measured can be defined by

$$\sigma(E_{\mathrm{min}}, E_{\mathrm{max}}) = \int_{E_{\mathrm{min}}}^{E_{\mathrm{max}}} \frac{d\sigma}{dE_\gamma} dE_\gamma, \tag{46}$$

where the differential cross section $d\sigma/dE_\gamma$ is given by Eq. (5). The $E_\gamma$ range is [5.0, 12.5] MeV for the incident energy $E_i = E_{\mathrm{res}}$ and [7.0, 14.5] MeV for $E_i = E_{\mathrm{off}}$ [13]. For the theoretical cross sections, the integration over $E_\gamma$ is limited to $E_i$ since $E_\gamma$ larger than $E_i$ is unphysical. When $E_\gamma$ tends to $E_i$, the final energy $E_f$ tends to zero. Consequently, the final wave function is damped by the Coulomb barrier and the differential bremsstrahlung cross section $d\sigma/dE_\gamma$ tends to zero. The integration in Eq. (46) is performed numerically.

Let us note that the differential cross section $d\sigma/dE_\gamma$ tends to infinity when the photon energy tends to zero. Very low photon energies would require treating bremsstrahlung and elastic scattering in a common framework [50]. However, in practice, this problem is avoided since the lower limit of the photon energy detection $E_{\mathrm{min}}$ is large enough in the considered experiments.

The experimental and theoretical cross sections are compared in Table I. Experimental errors include statistical and systematic errors. Both approaches lead to results in agreement with the experimental data. The Siegert results are, however, smaller than the non-Siegert ones by about 10% on resonance and 20% off resonance. They seem to be closer to experiment. To evaluate the importance of the $4^+$ to $2^+$ transitions, cross sections considering only these transitions are given in parentheses in Table I. At the resonance energy $E_{\mathrm{res}}$, the $4^+$ to $2^+$ transitions are actually dominant. Their contribution to the total cross section is about 90%. Off resonance, their relative importance is weaker. Their contribution is smaller than 50%.

Other values of the initial energy are also considered. The integrated cross sections for both $E_\gamma$ ranges are shown in Fig. 3 as a function of the initial energy $E_i$. Integrated bremsstrahlung cross sections were already calculated in a potential model but considering separately the transitions to the $0^+$ states [51] and the transitions to the $2^+$ states [52]. Moreover, the $E_\gamma$ range was not the same as the experimental one which does not enable a direct comparison.

Again, results obtained with the Siegert approach and its null-current approximation are nearly identical. Relative differences between cross sections at the two considered values of the channel radius are smaller than 1% and absolute differences are smaller than 1.6 nb. For all considered energies, differences between the Siegert approach and its null-current

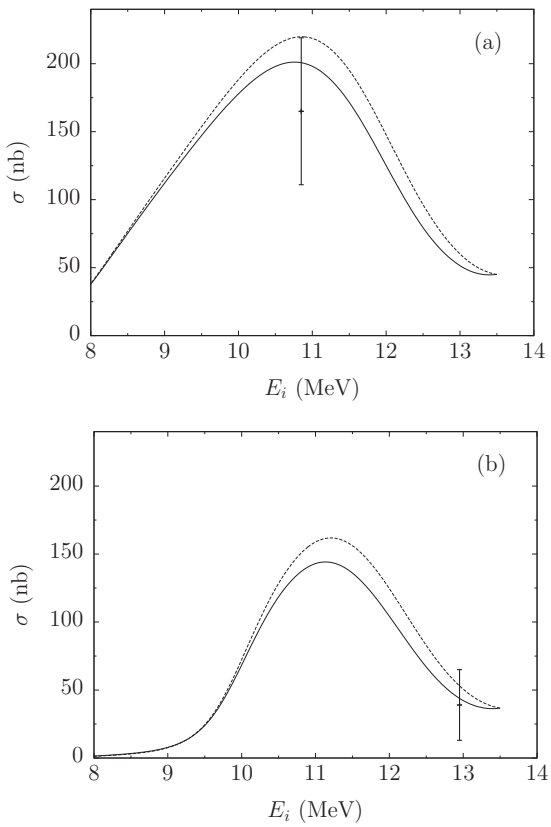


FIG. 3. Cross sections $\sigma(E_{\min}, E_{\max})$ as a function of the initial energy $E_i$ for (a) $[E_{\min}, E_{\max}] = [5.0, 12.5]$ MeV and (b) $[E_{\min}, E_{\max}] = [7.0, 14.5]$ MeV. Full lines correspond to the Siegert operator $\mathcal{M}^{\mathrm{E(S)}}_{\lambda\mu}$ and dashed lines to the non-Siegert operator $\mathcal{M}^{\mathrm{E}}_{\lambda\mu}$. The null-current approximation $\mathcal{M}^{\mathrm{E}(J=0)}_{\lambda\mu}$ is indistinguishable from the full lines. Experimental data come from Ref. [13].

approximation are totally negligible. The differences between the Siegert and non-Siegert approaches remain weak in comparison with the experimental error bars.

The $E_\gamma$ range has a rather large influence on the integrated cross sections. Comparing theoretical and experimental results thus requires using the same $E_\gamma$ range. This point was overlooked in Ref. [13].

## IV. CONCLUSION

Previous microscopic models of nucleus-nucleus bremsstrahlung totally neglected the contribution of the meson exchange currents to the photon-emission operator. In this work, a microscopic cluster model of bremsstrahlung is developed which implicitly takes them partially into account by using an extension of the Siegert theorem. The photon-emission operator is deduced from the nuclear density rather than from the nuclear current. Strictly speaking, the nuclear current dependence is not totally canceled, but the results show that this residual dependence is negligible for the $\alpha(\alpha, \alpha\gamma)\alpha$ reaction.

In addition to this implicit inclusion of the meson exchange currents, the Siegert photon-emission operator has the advantage over the non-Siegert one of leading to less complicated calculations. Consequently, considering the Siegert photon-emission operator will make easier the development of *ab initio* bremsstrahlung models.

The microscopic cluster model is applied to the $\alpha + \alpha$ bremsstrahlung for an effective NN interaction. Differences between cross sections obtained with the Siegert and non-Siegert approaches increase with the photon energy. They are quite weak for photon energies limited to 5 MeV but start to become important for photon energies around 10 MeV. A good agreement is obtained with the experimental data of Ref. [13] about on- and off-resonance $4^+ \to 2^+$ transitions, but the error bar is too large to clearly discriminate the Siegert and non-Siegert approaches.

It will be interesting to apply the microscopic cluster model to other low-energy reactions involving light nuclei. A first test on $\alpha$+nucleon bremsstrahlung, where $E1$ transitions are not forbidden, would be an important step to prepare *ab initio* studies of the $t(d, n\gamma)\alpha$ reaction. It should also be possible to extend microscopic cluster-model descriptions to proton scattering on $^{12}$C or $^{16}$O for which experimental data exist at low energies [53–57].

## ACKNOWLEDGMENTS

We thank P. Descouvemont and S. Quaglioni for useful discussions and V. Datar for the communication of some experimental details. This text presents research results of the interuniversity attraction pole program P7/12 initiated by the Belgian-state Federal Services for Scientific, Technical and Cultural Affairs. J.D.E. acknowledges support from the F.R.S.-FNRS.

## APPENDIX: APPLICATION OF THE CONTOUR INTEGRATION METHOD

In this Appendix, a variant of the contour integration method proposed in Ref. [45] is presented and applied, as an illustration, to the calculation of the integral

$$\int_a^\infty \rho^2 g_{\mathrm{ext}}^{l_f *} g_{\mathrm{ext}}^{l_i} j_\lambda(k\rho) d\rho, \tag{A1}$$

which appears in Eq. (40).

The integration range is first divided in two: from $a$ to $\rho_R$ and from $\rho_R$ to infinity. The second integral is written after some algebraic manipulations as a function of the incoming and outgoing Coulomb wave functions,

$$\begin{aligned}
&\int_{\rho_R}^\infty \rho^2 g_{\mathrm{ext}}^{l_f *} g_{\mathrm{ext}}^{l_i} j_\lambda(k\rho) d\rho \\
&= 2(1+\delta_{12})\pi \frac{\sqrt{(2l_i+1)(2l_f+1)}}{k_i k_f \sqrt{v_i v_f}} e^{i(\delta_{l_i}+\sigma_{l_i}-\delta_{l_f}-\sigma_{l_f})} i^{l_i - l_f} \\
&\quad \times \mathrm{Im}\left\{ i \int_{\rho_R}^\infty O_{l_i}(\eta_i, k_i\rho) e^{i\delta_{l_i}} j_\lambda(k\rho) \right. \\
&\quad \left. \times \left[ I_{l_f}(\eta_f, k_f\rho) e^{-i\delta_{l_f}} - O_{l_f}(\eta_f, k_f\rho) e^{i\delta_{l_f}} \right] d\rho \right\},
\end{aligned} \tag{A2}$$

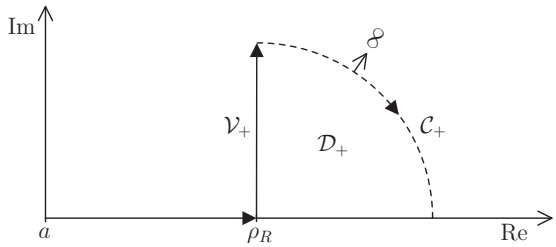


FIG. 4. Schematic view of the contour integration method.

where $O_l$ an $I_l$ are the outgoing and incoming Coulomb wave functions defined by

$$O_l(\eta, x) = G_l(\eta, x) + i F_l(\eta, x), \tag{A3}$$

$$I_l(\eta, x) = G_l(\eta, x) - i F_l(\eta, x). \tag{A4}$$

The dominant part of the oscillating terms in the integral in Eq. (A2) behaves asymptotically as

$$e^{i(k_i \pm k_f \pm k)\rho}. \tag{A5}$$

Since $k_i$ is larger than $k_f$ and much larger than $k$ (which is proportional to $k_\gamma$), the sign of the imaginary exponential in Eq. (A5) is positive. This property is used in the choice of the contour integration. The integral in Eq. (A2) can be written as a sum of integrals in the complex plane,

$$\int_{\rho_R}^{\infty} f(\rho)d\rho = \int_{\mathcal{V}_+} f(z)dz + \int_{\mathcal{C}_+} f(z)dz - \oint_{\mathcal{D}_+} f(z)dz, \tag{A6}$$

where the function $f$ is defined by

$$f(\rho) = O_{l_i}(\eta_i, k_i\rho)e^{i\delta_{l_i}} j_\lambda(k\rho) \times [I_{l_f}(\eta_f, k_f\rho)e^{-i\delta_{l_f}} - O_{l_f}(\eta_f, k_f\rho)e^{i\delta_{l_f}}] \tag{A7}$$

and the integration contours are shown in Fig. 4. Since the function $f$ has no pole in $\mathcal{D}_+$, the integral of $f$ over the contour of $\mathcal{D}_+$ is null. When the radius of $\mathcal{D}_+$ tends to infinity, the integral of $f$ over $\mathcal{C}_+$ is null too, and Eq. (A6) is simplified as

$$\int_{\rho_R}^{\infty} f(\rho)d\rho = i\int_0^{\infty} f(z_+)dy, \tag{A8}$$

where $z_+ = \rho_R + iy$. The transformation defined by Eq. (A8) enables us to replace the imaginary exponentials of the initial integral with decreasing exponentials. Finally, the integral in Eq. (40) is given by

$$\begin{aligned}
&\int_a^{\infty} \rho^2 g_{\text{ext}}^{l_f *} g_{\text{ext}}^{l_i} j_\lambda(k\rho)d\rho \\
&= \int_a^{\rho_R} \rho^2 g_{\text{ext}}^{l_f *} g_{\text{ext}}^{l_i} j_\lambda(k\rho)d\rho \\
&\quad + 2(1+\delta_{12})\pi \frac{\sqrt{(2l_i+1)(2l_f+1)}}{k_i k_f \sqrt{v_i v_f}} e^{i(\delta_{l_i}+\sigma_{l_i}-\delta_{l_f}-\sigma_{l_f})} i^{l_i - l_f} \\
&\quad \times \text{Im}\int_0^{\infty} O_{l_i}(\eta_i, k_i z_+)e^{i\delta_{l_i}} j_\lambda(kz_+) \\
&\quad \times \left[O_{l_f}(\eta_f, k_f z_+)e^{i\delta_{l_f}} - I_{l_f}(\eta_f, k_f z_+)e^{-i\delta_{l_f}}\right]dy.
\end{aligned} \tag{A9}$$

The first integral can be evaluated efficiently by a Gauss-Legendre quadrature. To calculate the second integral, it is convenient to split the two terms in two separated integrals because they have different decreasing speeds. Each of these two integrals can be evaluated efficiently by a Gauss-Laguerre quadrature associated with a suitable scale factor.

The Coulomb functions for complex variables are evaluated by the subroutine COULCC from Ref. [58]. The parameter $\rho_R$ is chosen large enough so that the Coulomb functions converge fast when they are evaluated in the complex plane.


[1] P. Signell, in *Advances in Nuclear Physics*, Vol. 2, edited by M. Baranger and E. Vogt (Plenum, New York, 1969) p. 257.
[2] M. L. Halbert, in *Proceedings of the Symposium on Two-Body Force in Nuclei, Gull Lake, Michigan, 1971*, edited by S. M. Austin and G. M. Crawley (Plenum, New York, 1972), p. 53.
[3] K. Nakayama, Phys. Rev. C **39**, 1475 (1989).
[4] R. G. E. Timmermans, B. F. Gibson, Y. Li, and M. K. Liou, Phys. Rev. C **65**, 014001 (2001).
[5] Y. Li, M. K. Liou, W. M. Schreiber, and B. F. Gibson, Phys. Rev. C **84**, 034007 (2011).
[6] J. Hall, W. Wölfli, and R. Müller, Phys. Lett. **37B**, 53 (1971).
[7] W. Wölfli, J. Hall, and R. Müller, Phys. Rev. Lett. **27**, 271 (1971).
[8] G. A. Anzelon, I. Slaus, S. Y. Tin, W. T. H. Van Oers, R. M. Eisberg, M. Makino, C. N. Waddell, and M. B. Epstein, Nucl. Phys. A **255**, 250 (1975).
[9] M. Hoefman *et al.*, Phys. Rev. Lett. **85**, 1404 (2000).
[10] B. Frois, J. Birchall, C. R. Lamontagne, U. von Moellendorff, R. Roy, and R. J. Slobodrian, Phys. Rev. C **8**, 2132 (1973).
[11] U. Peyer, J. Hall, R. Müller, M. Suter, and W. Wölfli, Phys. Lett. **41B**, 151 (1972).
[12] F. Haas, A. Elanique, R. M. Freeman, C. Beck, R. Nouicer, D. L. Watson, C. Jones, R. Cowin, P. Lee, and Z. Basrak, Nuovo Cimento A **110**, 989 (1997).
[13] V. M. Datar, S. Kumar, D. R. Chakrabarty, V. Nanal, E. T. Mirgule, A. Mitra, and H. H. Oza, Phys. Rev. Lett. **94**, 122502 (2005).
[14] T. J. Murphy *et al.*, Rev. Sci. Instrum. **72**, 773 (2001).
[15] D. Baye, P. Descouvemont, and M. Kruglanski, Nucl. Phys. A **550**, 250 (1992).
[16] P. Navrátil and S. Quaglioni, Phys. Rev. Lett. **108**, 042503 (2012).
[17] K. Nakayama and G. F. Bertsch, Phys. Rev. C **36**, 1848 (1987).
[18] I. V. Kopytin, M. A. Dolgopolov, T. A. Churakova, and A. S. Kornev, Phys. At. Nucl. **60**, 776 (1997).
[19] S. P. Maydanyuk, J. Phys. G: Nucl. Part. Phys. **38**, 085106 (2011).
[20] S. P. Maydanyuk, Phys. Rev. C **86**, 014618 (2012).
[21] D. Baye, C. Sauwens, P. Descouvemont, and S. Keller, Nucl. Phys. A **529**, 467 (1991).
[22] H. Feshbach and D. R. Yennie, Nucl. Phys. **37**, 150 (1962).
[23] D. Baye and P. Descouvemont, Nucl. Phys. A **443**, 302 (1985).
[24] Q. K. K. Liu, Y. C. Tang, and H. Kanada, Phys. Rev. C **41**, 1401 (1990).
[25] Q. K. K. Liu, Y. C. Tang, and H. Kanada, Phys. Rev. C **42**, 1895 (1990).

[26] Q. K. K. Liu, Y. C. Tang, and H. Kanada, Few-Body Syst. **12**, 175 (1992).
[27] K. Langanke, Phys. Lett. B **174**, 27 (1986).
[28] Q. K. K. Liu, Nucl. Phys. A **550**, 263 (1992).
[29] P. Descouvemont and D. Baye, Phys. Lett. **169B**, 143 (1986).
[30] P. Descouvemont, Phys. Lett. B **181**, 199 (1986).
[31] A. J. F. Siegert, Phys. Rev. **52**, 787 (1937).
[32] K.-M. Schmitt, P. Wilhelm, H. Arenhovel, A. Cambi, B. Mosconi, and P. Ricci, Phys. Rev. C **41**, 841 (1990).
[33] H. J. Rose and D. M. Brink, Rev. Mod. Phys. **39**, 306 (1967).
[34] A. Bohr and B. R. Mottelson, *Nuclear Structure*, Vol. 1 (Benjamin, New York, 1969).
[35] A. Messiah, *Mécanique Quantique*, Vol. 2 (Dunod, Paris, 1962).
[36] J. L. Friar and S. Fallieros, Phys. Rev. C **29**, 1645 (1984).
[37] D. Baye, Phys. Rev. C **86**, 034306 (2012).
[38] H. Horiuchi, Prog. Theor. Phys. Suppl. **62**, 90 (1977).
[39] Y. C. Tang, in *Topics in Nuclear Physics II*, Lecture Notes in Physics Vol. 145, edited by T. T. S. Kuo and S. S. M. Wong (Springer, Berlin, 1981), p. 571.
[40] D. Baye, P.-H. Heenen, and M. Libert-Heinemann, Nucl. Phys. A **291**, 230 (1977).
[41] P. Descouvemont and D. Baye, Rep. Prog. Phys. **73**, 036301 (2010).
[42] D. Baye and P. Descouvemont, Nucl. Phys. A **407**, 77 (1983).
[43] P.-O. Löwdin, Phys. Rev. **97**, 1474 (1955).
[44] D. Brink, in *Proceedings of the International School Enrico Fermi 36, Varenna 1965*, edited by C. Bloch (Academic, New York, 1966), p. 247.
[45] C. M. Vincent and H. T. Fortune, Phys. Rev. C **2**, 782 (1970).
[46] R. J. Philpott and D. Halderson, Nucl. Phys. A **375**, 169 (1982).
[47] D. R. Thompson, M. LeMere, and Y. C. Tang, Nucl. Phys. A **286**, 53 (1977).
[48] R. Kamouni and D. Baye, Nucl. Phys. A **791**, 68 (2007).
[49] V. M. Datar ( private communication).
[50] J. D. Bjorken and S. D. Drell, *Relativistic Quantum Mechanics* (McGraw-Hill, New York, 1964).
[51] K. Langanke and C. Rolfs, Phys. Rev. C **33**, 790 (1986).
[52] K. Langanke and C. Rolfs, Z. Phys. A - Atomic Nuclei **324**, 307 (1986).
[53] C. C. Trail, P. M. S. Lesser, A. H. Bond, M. K. Liou, and C. K. Liu, Phys. Rev. C **21**, 2131 (1980).
[54] P. M. S. Lesser, C. C. Trail, C. C. Perng, and M. K. Liou, Phys. Rev. Lett. **48**, 308 (1982).
[55] D. Yan, P. M. S. Lesser, M. K. Liou, and C. C. Trail, Phys. Rev. C **45**, 331 (1992).
[56] A. D'Arrigo, N. Doroshko, N. Eremin, G. Giardina, B. Govorov, V. Olkhovsky, and A. Taccone, Nucl. Phys. A **549**, 375 (1992).
[57] A. D'Arrigo, N. Doroshko, N. Eremin, G. Fazio, G. Giardina, B. Govorov, V. Olkhovsky, and A. Taccone, Nucl. Phys. A **564**, 217 (1993).
[58] I. J. Thompson and A. R. Barnett, Comput. Phys. Commun. **36**, 363 (1985).